SAF for Land Surface Analysis (LSA SAF)
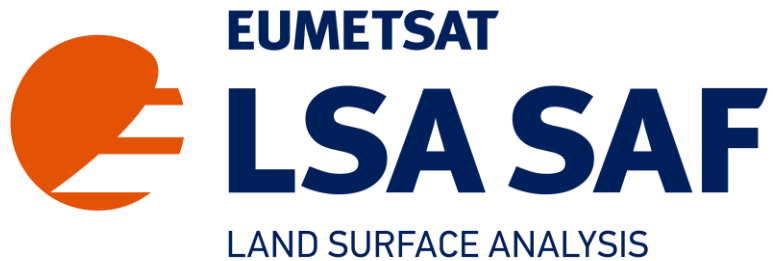

Algorithm Theoretical Basis Document

Meteosat Second Generation based products:

Instantaneous evapotranspiration	**(MET v2)**
Daily evapotranspiration	**(DMET v2)**
Surface latent heat flux	**(LE)**
Surface sensible heat flux	**(H)**

DOCUMENT SIGNATURE TABLE

	Name	Date	Signature
Prepared by:	RMI Team	25/11/2016	
Approved by:	Land SAF Project Manager (IPMA)		

DOCUMENTATION CHANGE RECORD

Issue / Revision	Date	Description:
Version 1.0	12/11/2015	Version submitted to SG for ORR-ET (12 11 2015)
Verson 1.1	25/11/2016	Version with PCR reviewers comments (1-16/11/2016)

TABLE OF CONTENTS

1   Introduction

The evapotranspiration (ET) algorithm developed in the framework of the Satellite Application Facility on Land Surface Analysis, LSA-SAF (Trigo et al., 2011), targets the quantification of the flux of water vapour and heat release from the ground surface (soil and canopy) into the atmosphere using input data derived from Meteosat Second Generation (MSG) satellites. The present document aims at describing the methodology adopted for the LSA-SAF ET algorithm, used for the generation of half-hourly MET and daily DMET products, version 2, and the half-hourly latent (LE) and sensible heat fluxes (H).

Satellite remote sensing (SRS) stays as the only method capable of providing wide area coverage of environmental variables at economically affordable costs. However, a major difficulty to the use of SRS for monitoring ET is that the phase change of water molecules produces neither emission nor absorption of an electromagnetic signal. Therefore, ET process is not directly quantifiable from satellite observations at regional and global scale. It has to be assessed, taking advantage of information gained through the satellite about surface variables influencing evapotranspiration (Choudhury, 1991). Most of proposed methods use SRS derived data combined into models with different degrees of complexity ranging from empirical direct methods to complex deterministic models based on Soil-Vegetation-Atmosphere Transfers (SVAT) modules that compute the different components of the energy budget (Courault et al., 2005; Verstraeten et al., 2008; Wang and Dickinson, 2012; Petropoulos, 2013; Liou and Kumar Kar, 2014). Empirical methods are only applicable locally, where they were calibrated. Another class of models includes surface energy balance models, such as SEBS (Su, 2002), which solve the energy balance at the surface using the energy components derived from the satellite. Most remote sensing methods can only be applied for clear sky conditions.

The methodological approach selected in the framework of the LSA-SAF intends to be applicable at regional to global scales, to be able to provide a monitoring at short time step to follow the diurnal cycle evolution and to obtain results continuously for all nebulosity conditions. In addition, it has been conceived to ingest an increasing number of remote sensing derived products as they are released through time. The adopted method can be described as a SVAT scheme reduced to its diagnostic components and modified to accept input data from external sources in near-real time (Ghilain et al., 2011). It is based on the physics of the Tiled ECMWF Surface Scheme for Exchange Processes over Land, TESSEL (Viterbo and Beljaars, 1995; van den Hurk et al., 2000) and H-TESSEL (Balsamo et al, 2009; Albergel et al, 2012). Main modifications operated to the initial model allow the model to run decoupled from the atmospheric model and from the soil heat and water diffusion modules, as well as to use data from external sources like SRS derived data, Numerical Weather Prediction model (NWP) output and information about land-cover characteristics. The parameterization has been slightly modified or re-calibrated, and features added. The adopted methodology combines the forces of remote sensing approaches and NWP models. In this approach, the area for which ET has to be assessed is divided into independent pixels, in a one-to-one correspondence with the pixels of a satellite image. Each pixel is in turn considered as being a mix of homogeneous *tiles*, each tile representing a particular soil surface: bare soil, short canopy, high canopy, *etc*. The global pixel value is obtained through the weighted contribution of each tile. Theoretically, ET can be derived in near-real time at the time resolution of MSG satellite images (timeliness of 3 hours from the image acquisition, see Product Requirement Document). In practice, the generation of

ET will be limited by the availability of input data. Since radiation components from LSA-SAF are generated every 30 minutes, LSA-SAF MET is produced at the same frequency.

The next section describes the methodology, with the detailed description of the model used, the physical equations, parameterisation, assumptions, and algorithm details. A short description of the model output is then presented. Expert knowledge about the global ET product quality and its added value is provided in a final section.

2   The LSA-SAF evapotranspiration algorithm

The algorithm used for the generation of MET v2, DMET v2, LE and H products makes use of LSA-SAF products to deliver maps over the full field of view of MSG (South America, Europe, Africa and Middle East) at the variable spatial resolution of Meteosat Second Generation satellites, 3.1 km at sub-satellite point (Table 1).

Table 1: List of input data of the LSA-SAF ET v2 algorithm, their source and frequency. SRS stands for satellite remote sensing and NWP for numerical weather forecasts. In squared bracket input variable means potential use depending on the technical capabilities of the operational networking environment. The detail use of the variables and products are detailed further in the text.

Input	Variable used	Source	Provider	Product	Frequency
Radiative forcing	Shortwave radiation $S_\downarrow$	SRS	**LSA-SAF**	**DSSF**	30 min
	Longwave radiation $L_\downarrow$		**LSA-SAF**	**DSLF**	30 min
	Surface albedo α		**LSA-SAF**	**AL-BB-BH**	1 day
	Fire radiative Power FRP		**LSA-SAF**	**FRP-Pixel**	15 min
Meteorological fields	Air temperature, humidity, pressure and wind speed T_a, q_a, P_a, U_a	NWP	ECMWF IFS	**2T, 2D, SLP, 10U, 10V**	3 hours
Land cover	Tile %	SRS	ECOCLIMAP-II		Static
	Snow	SRS	**H-SAF**	**SC2**	1 day
Biophysical parameters	Leaf area index LAI, Fraction of vegetated cover F$_v$	SRS	**LSA-SAF**	**LAI FVC**	1 day
Soil moisture	Soil water content in 4 soil layers θ_k	NWP	ECMWF IFS	**SWVL**	3 hours
	[Soil water Index θ_k	SRS	**H-SAF**	**H-SAF H14 (SM-DAS-2)**	1 day]
	Land surface temperature LST	SRS	**LSA-SAF**	**LST**	15 min

The LSA-SAF ET v2 algorithm is composed of three major software units: 1) a preprocessing module, in which various input variables derived from the satellites or from other sources are transformed to physical variables directly useable by the model unit, 2) the physical model unit, which derive the instantaneous physical variables related to evapotranspiration and surface heat fluxes from the given input and 3) a post-processing module, in which the daily product is created. The pre-processing module is operated once at beginning of each day, the second every time radiations components are issued (LSA-SAF, 30 minutes) and the post-processing module at the end of each day.
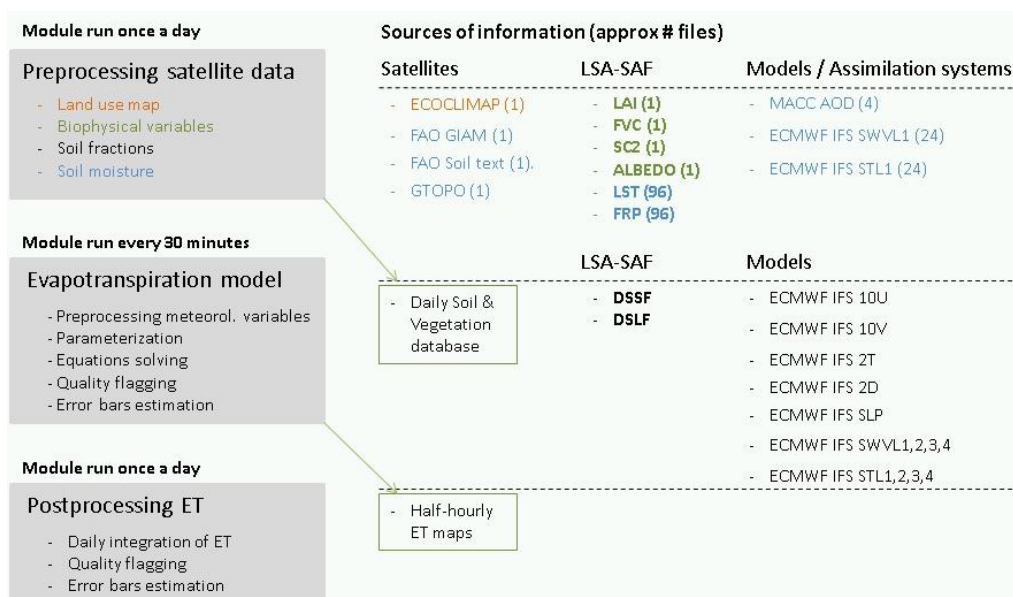
Figure 1: Description of the three successive modules, tasks and input to produce instantaneous surface heat fluxes, evapotranspiration and daily evapotranspiration. Acronyms are listed at the end of the document. For each module, the information ingested from the different sources are listed on the right.

The elementary spatial unit of the algorithm is called *pixel* in reference to the basic unit of the SEVIRI instrument on board of MSG satellites. The dimension of the surface represented by a pixel varies in function of its location (longitude and latitude) and is 3.1x3.1 km² at MSG sub-satellite point. The size of a pixel over the European region is about 4x5 km². Since the vegetation cover influences most of the surface atmospheric processes over land, the estimation of ET is made by reference to a land cover map which provides the fraction of vegetation types within each MSG pixel.

The different vegetation types considered in the MET algorithm are listed in Table 2. This primary vegetation types are called "tiles" and each pixel may be composed of several tiles. In practice, a maximum of four tiles (the dominant between the different vegetation types, surface water, inland water, permanent snow, bare soil, rocks and cities) are considered by pixel. ET is calculated separately for each tile in pixel and the pixel value is obtained by a weighted contribution of all tiles composing the pixel.

Figure 2 Example of a pixel unit composed of different tiles: forest, grass, crops and bare soil.

In case of snow events on the vegetated or non vegetated surfaces, the less dominant tile is dropped to leave space for the snow tile.

#	Surface type	$r_{s,min}$ [s/m]	g_D [hPa^{-1}]	β_l [kg. MJ^{-1}]
1	Bare soil	250	-	-
2	Snow	-	-	-
3	Deciduous Broadleaved trees	350	0.03	0.49/*1.55*
4	Evergreen Needleleaved trees	180	0.03	0.49/*1.55*
5	Evergreen Broadleaved trees	250	0.03	0.96
6	Crops (2 types)	180	0	0.29/*0.13*
7	Irrigated crops	180	0	0.29/*0.13*
8	Grass (2 types)	110	0	0.78/*0.26*
9	Bogs and Marshes	250	0	5.87
10	Rocks	1000	-	-
11	Open water	0	-	-
12	City	1000	-	-

Table 2 Surface type considered by the algorithm and associated parameters rs$_{min}$ (minimum stomatal resistance), g$_D$ (coefficient for the dependency of canopy resistance on water vapour pressure deficit) and β$_l$, the conversion factor linking fire radiative power and dry matter combustion rate for each class (adapted from Kaiser et al, 2012).

2.1 Pre-processing satellite data

The pre-processing unit of the algorithm aims at providing, daily, information on surface cover, associated parameters, and soil moisture status to the evapotranspiration model. It is processed once a day after the production of the daily LSA-SAF LAI and AL. It makes use of static input information and several products from satellite remote sensing (LSA-SAF, Hydrology (H)-SAF) and numerical weather predictions (ECMWF).

Static input file   The static input file provides the algorithm a land cover map (ECOCLIMAP-II (Masson et al., 2003; Faroux et al, 2013) aggregated to SEVIRI resolution and complemented by the Food and Agriculture Organization (FAO) lithology map) that contains the fraction of each tile within every pixel, a 10 days climatology of LSA-SAF LAI and AL, with their associated uncertainty bar, and a mask to indicate to the algorithm the soil moisture input to be used. In addition, maps of local extrema of surface morning heating rates and the per-pixel parameters to make ECMWF IFS SWVL1 or H-SAF H14 SSM compatible with other sources are provided. (We give details of the processing of this static input file prepared at the Royal Meteorological Institute of Belgium in Annex A).

Daily pre-processing of satellite data

Land cover map and snow   The LSA-SAF snow cover product is checked daily to eventually update the percentages of tiles provided by the land cover map (Figure 3). If the land cover map indicates permanent snow, the product is not checked. Depending on the snow cover (total/partial), the fraction of snow assigned for the pixel is set to 100% or 50%, the fraction of the other remaining tiles being re-scaled to the complement. An albedo of 0.9 is assigned to snow tiles.

Biophysical variables   The daily LAI and AL products are assimilated using optimal interpolation with the 10-days climatology of the static file. Tile estimates of LAI are obtained by applying a least-square algorithm on a spatial window of 9 pixels around each considered pixel. It takes into account the LAI values of each pixel and the respective percentage of vegetation tiles, under the assumption of null LAI over bare soil fraction. Because of probable inconsistencies between tile percentages from ECOCLIMAP land cover map and LSA-SAF

LAI, spurious tile LAI may be estimated for tiles with low cover fraction. In those cases, the tile LAI are corrected with the value of the ECOCLIMAP tile LAI. The correction considers an adaptative weight, decreasing the tile value contribution linearly with its occupation fraction. A detailed description of the methodology can be found in Ghilain et al (2012). The fraction of bare soil is adapted depending on the surface type: forests tiles and perennial grasslands are considered to be composed of 80% of full vegetation cover and 20% of bare soil, while crops and non perennial grasslands (class determined on the basis of the land cover map and the soil moisture mask) will have a vegetation cover varying between 0 and 100% along a year, with a fraction linearly deduced from the range of LAI values. The land cover map is therefore again adapted such as to add up all the bare soil contribution together. For each separate tile, a roughness length for momentum (z_{om}) and heat (z_{oh}) is computed from LAI and a tree height map (Simart et al, 2011) following ECOCLIMAP relations. A land emissivity is computed pixelwise following the ECOCLIMAP relation (linear weighted contribution of 0.96 for bare soil and 0.99 for vegetated surfaces) feeded by the daily fraction of vegetation produced by LSA-SAF.
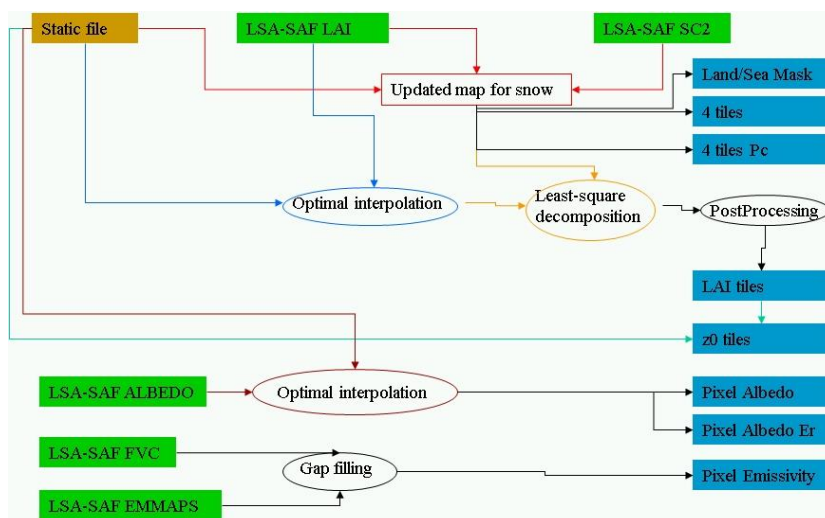
Figure 3: Flowchart of the creation of daily tile proportions, LAI, albedo, emissivity and surface roughness lengths within the daily pre-processing unit.

Soil moisture input production The soil moisture mask from the static input file indicates whether to use satellite derived from the satellite or from numerical weather predictions. In the case satellite data is the preferred source, the algorithm computes the surface soil moisture index from the morning heating rates (HR) using LSA-SAF LST (Ghilain et al., 2015, 2016). In case satellite observations are missing, due for example to persistent cloud cover over the morning, ECMWF SSM (ECMWF IFS SWVL1 or H-SAF H14 SSM, depending on the choice made for the operational processing chain) is transformed using the scaling parameters from the static input file to match the overall behaviour of the satellite retrieval of soil moisture. If numerical weather prediction is the preferred input, the ECMWF SSM is propagated as it and if the two sources are equally advised, half of the weight is assigned for each input and averaged. The merged map obtained is flagged using a priori knowledge from the input quality, aerosol loads (derived from the aerosol optical depth from the Copernicus Atmospheric Monitoring Service, MACC AOD) and presence of fire (by means of fire radiative power product, LSA-SAF FRP-Pixel). Finally, if satellite data is selected, the information is propagated to the root-zone by means of an exponential filter with a characteristic decay time of 1 day for short vegetation types and 15 for high ones. If ECMWF is selected, then root-zone soil moisture is computed from the soil moisture estimated for the 4 soil layers.

In that case, the averaged soil water content in the root-zone is obtained by averaging the four-layered soil moisture (Eq 1), modulated by a function of soil temperature to take in account the phase of the water in the soil (Eq 2) and is combined in a weighted average value, using the plants roots distribution in soil (Table 3). If the source is H-SAF SM-DAS-2 (H14), the soil moisture index is only averaged with respect to root distribution, as it represents already only the water in liquid phase in the soil (H14 ATBD).

$$\bar{\theta} = \sum_{k=1}^{4} R_k . \max(f_{liq,k} . \theta_k , \theta_{pwp})$$

(1)

$$f_{liq,k} = \begin{cases} 1 & \text{if } T_k > T_{f1} (=274.15 \text{ K}) \\ 1 - 0.5 . \left\{ 1 - \sin\left[\dfrac{\pi.(T_k - 0.5.T_{f1} - 0.5.T_{f2})}{T_{f1} - T_{f2}} \right] \right\} & \text{if } T_{f2} \le T_k \le T_{f1} \\ 0 & \text{if } T_k \le T_{f2} (=270.15 \text{ K}) \end{cases}$$

(2)

Table 3 Roots distribution (R_k) per vegetation type (in %) over the four soil layers. Vegetation types are listed in Table 2.

Tile	1	2	3	4	5	6	7	8	9	10	11	12
R_1	100	-	24	26	25	24	24	35	25	-	-	-
R_2	0	-	38	39	34	41	41	38	34	-	-	-
R_3	0	-	31	29	27	31	31	23	27	-	-	-
R_4	0	-	7	6	14	4	4	4	11	-	-	-

Figure 4: Flowchart of the generation of daily soil moisture estimates (surface and root-zone) within the daily pre-processing unit. TIR data refers to the use of LSA-SAF LST. CDF matching (cumulative distribution function) makes use of static parameters to make ECMWF surface soil moisture (SSM)

compatible with LST derived soil moisture. Specific estimation is applied for if the maximum LAI of the pixel over the year (LAI_max) is larger than the defined threshold (T).
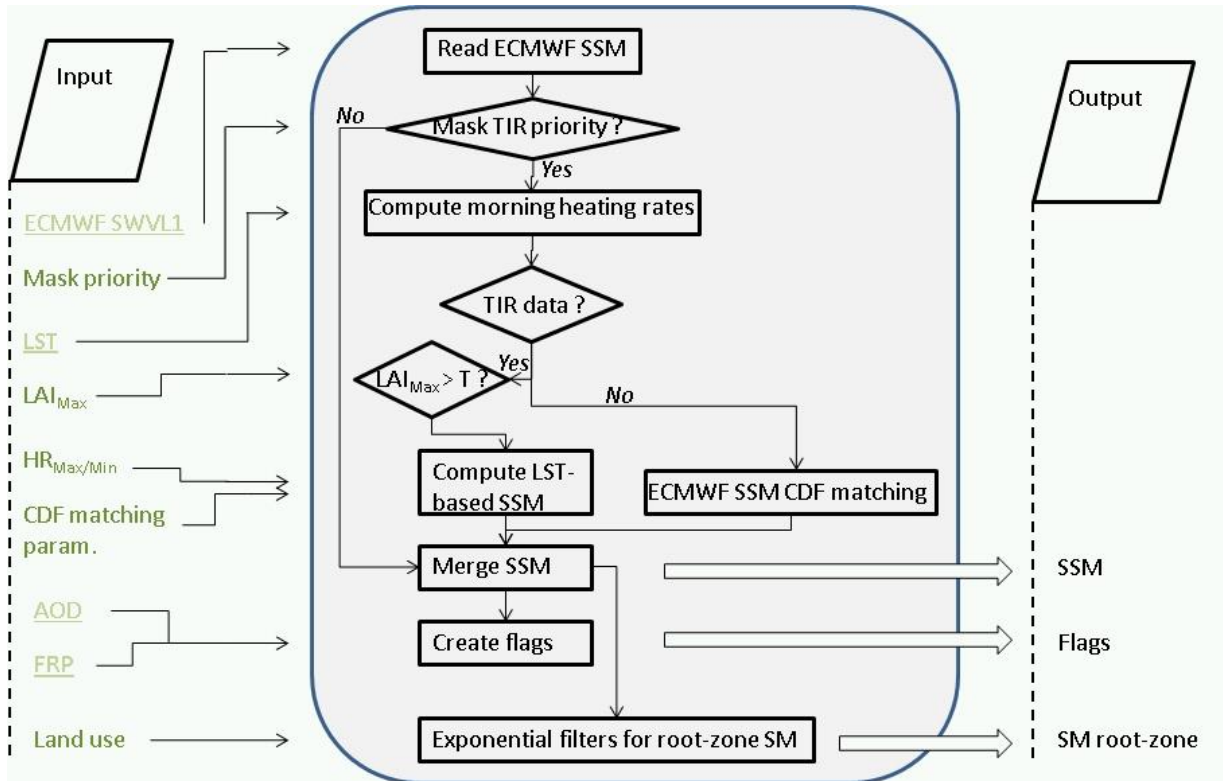
Note here that the time lag between the baseline soil moisture available for the evapotranspiration algorithm and the actual time can be more than 1 day at some period of the day, and depending on the processing time of the module. The preferred time for Europe and Africa is around 14:30 UTC of day D, so that H14 product averaging soil moisture of day D-1 and LSA-SAF LST for day D are available, and therefore new baseline soil moisture can be input the LSA-SAF ET v2 algorithm from 15 UTC onwards.

2.2 The physical evapotranspiration model

The surface energy balance is computed by the algorithm at tile level in a conceptual layer, called *skin* layer. This latter represents the coverage of the land surface (vegetation, bare soil, snow) as a flat layer, without description of the 3-D structure of the canopy.

The physical model aims at computing, for each tile i in the considered pixel, the partition of net radiation (R_{ni}) between sensible and latent heat flux (H_i, LE_i) and heat conduction into the ground (G_i) (Eq 3).

$$Rn_i = H_i + LE_i + G_i \qquad (3)$$

The land cover influences the repartition of the surface fluxes and the forcing fields used in the model. The main input data are solar radiation at surface ($S_\downarrow$), long-wave radiation at surface ($L_\downarrow$), air temperature (T_a) and specific humidity (q_a) at reference height (z_a), surface air pressure (P_a), wind speed (U_a) at reference height (z), surface albedo (α), soil temperature

(T_k) and soil moisture (θ_k) at four soil depths (k). Some of the input data are provided by the pre-processing unit, a file being generated once a day.

Preparation of input information

Meteorological auxiliary data needed by the evapotranspiration model are retrieved from short-term ECMWF deterministic forecasts from numerical weather predictions (ECMWF IFS). These data gathered at the original spatial resolution (e.g. 0.25°x0.25° in 2010, 0.1°x0.1° in 2016) are mapped onto the MSG grid, spatially and temporally (from 3 to 1 hour) linearly interpolated and eventually corrected in a pre-processing toolbox operated at LSA-SAF common to different algorithms (eg. the 2-m air temperature is corrected for topography). The interpolated meteorological fields provided are the 2-m air temperature, the 2-m dew point temperature, the 10-meters wind speed, the surface atmospheric pressure, the soil moisture and soil temperature in the four soil layers. Dew point temperature and air pressure are used to calculate air specific humidity. Soil water contents for the 3 deepest soil layers are rescaled from the initial wilting points and field capacity values to a uniform range for an average soil $(0.171 - 0.323 \text{ m}^3.\text{m}^{-3})$. For the soil water content of the first soil layer, a rescaling is performed: the actual minimum value of surface soil moisture from ECMWF IFS for each pixel (determined over an analysis of 2 years), if lower than wilting point, must correspond to the wilting point defined in the LSA-SAF ET algorithm, such as it is compatible with the parameterization. In case H-SAF SM-DAS-2 is used, zero is interpreted as the minimum soil moisture (or wilting point, in the model).

A gap filling procedure is applied on DSLF product by a spatial interpolation of values around the missing pixel values, if present and for areas of small extent.

Energy balance

The net radiation is given by the net balance between shortwave and longwave radiation components reaching and leaving the land surface (Eq 4).

$$R_n = (1-\alpha)S_\downarrow + \varepsilon(L_\downarrow - \sigma T_{sk,i}^4)$$

ε is the surface emissivity,
$T_{sk,i}$ is the skin temperature (K),[1]
σ the Stefan-Boltzmann cst $(=5.67\ 10^{-8}\text{ W m}^{-2}\text{ K}^{-4})$. (4)

A common choice to parameterize the soil heat flux is to approximate it as a fraction of the net surface radiation, assuming that it has a diurnal variation in phase with the net radiation. While different variants based on the same assumption exist in the literature (Choudhury et al., 1987; Bastiaansen, 1995; Norman et al., 1995; Jacobsen and Hansen, 1999; Friedl, 2002; Kustas et al., 1993; Su, 2002; Santanello and Friedl, 2003), we choose the parameterization of Chebhouni et al. 1996 (Eq 5), and is adapted for specific land types.

$$G_i = \beta_i.R_{n_i} \qquad \text{where } \beta_i = 0.5.\exp(-2.13.(0.88-0.78.\exp(-0.6.LAI_i))),$$ (5)
except for rocks, snow and inland water where β_i = 0.15, 0.05 and 0.10, respectively.

---

[1] The skin temperature is computed by the evapotranspiration model by an iterative method described later.

The latent and sensible heat fluxes are obtained via a resistance approach, combining a response of the stomata closure by environmental stress (canopy resistance) and the aerodynamic resistance (Eqs 6 & 7).

$$LE_i = \frac{L_v \rho_a}{(r_{a_i} + r_{c_i})} \left[q_{sat}(T_{sk,i}) - q_a(T_a) \right]$$

ρ_a is the air density,

r_a the aerodynamic resistance,

z_a is the air temperature measurement height (= 2 m), (6)

z is the wind speed measurement height (=10 m),

$$H_i = \frac{\rho_a}{r_{a_i}} \left[c_p(T_{sk,i} - T_a) - g z_a \right]$$

r_c is the canopy resistance,

q_a the specific humidity, (7)

q_{sat} the specific humidity at saturation.

Aerodynamic resistance

The aerodynamic resistance (r_{a_i}) is directly connected to the stability of the atmosphere, friction velocity (u_{*_i}) and Obukhov length (L_i) are therefore needed to calculate it. In Eqs 8-10 Ψ_h and Ψ_m are, respectively, the sensible heat and momentum stability functions (Beljaars and Viterbo, 1994). Sensible and latent heat fluxes are needed in equation 10 to compute the Obukhov length, the complete system of non-linear equations has to be solved iteratively (see section 2.2 for solving procedure). During the iterative process, the aerodynamic resistance has been limited to 100 s.m^{-1}, which leads to better estimates of Tskin compared to LSA-SAF LST during night (Martins et al, 2016), without affecting LE values.

$$\frac{1}{r_{a_i}} = \frac{k u_{*i}}{\ln\left(\frac{z_a - d_i}{z_{0hi}}\right) - \Psi_h\left(\frac{z_a - d_i}{L_i}\right) + \Psi_h\left(\frac{z_{0hi}}{L_i}\right)} \quad (8)$$

$$u_{*_i} = \frac{k U_a}{\ln\left(\frac{z - d_i}{z_{0m_i}}\right) - \Psi_m\left(\frac{z - d_i}{L_i}\right) + \Psi_m\left(\frac{z_{0m_i}}{L_i}\right)} \quad (9)$$

$$L_i = \frac{\rho_a u_{*_i}^3}{k g \left(\frac{H_i}{c_p T_a} + 0.608 \frac{LE_i}{L_v}\right)}$$

(10)

Canopy resistance

The formulation canopy resistance r_c of the vegetation to transpiration is based on van den Hurk et al. (2000) (Eq 11), while the parameterization for crops and non perennial grasslands has been slightly changed, such as to introduce more sensitivity of the model for low green biomass conditions (Eq 11).

For crops and grass in semi-arid ecosystems:

$$r_c = \left(\frac{r_{s,min}}{0.25.(\exp(LAI) - 0.8)} + 50 \right) f_1(S_\downarrow) f_2(\bar{\theta}) f_3(D_a) \qquad (11)$$

$S_\downarrow$, surface shortwave radiation

$\bar{\theta}$, average unfrozen soil water content

D_a, atmospheric water pressure deficit

For the other cases:

LAI, leaf area index

$$r_c = \frac{r_{s,min}}{LAI} f_1(S_\downarrow) f_2(\bar{\theta}) f_3(D_a)$$

$r_{s,min}$, minimum stomatal resistance

The minimum stomatal resistance scaled by LAI or the effective LAI (crops and non-perennial grasslands) fixes the maximum rate of evapotranspiration observed for each vegetation type in absence of any constrains. Values of $r_{s,min}$ are recalibrated. The adopted values are listed in Table 2.

The Jarvis functions (van den Hurk et al , 2000) parameterize the dependency of the transpiration limitation to basic environmental variables. f_1 expresses the limitation due to the illumination of the active canopy (Eq 12), f_2 the limitation caused by a shortage of water in the soils (Eq 13) and f_3 the limitation for trees due to water vapour deficit in the atmosphere (Eq 14).

$$f_1(S_\downarrow)^{-1} = \min \left(1, \frac{b.S_\downarrow + c}{a.(b.S_\downarrow + 1)} \right) \qquad a=0.85, b=0.004, c=0.05 \qquad (12)$$

$$f_2(\bar{\theta})^{-1} = \begin{cases} 1 & \text{if } \theta_{cap} \geq \bar{\theta} \\ \dfrac{\bar{\theta} - \theta_{pwp}}{\theta_{cap} - \theta_{pwp}} & \text{if } \theta_{pwp} \leq \bar{\theta} \leq \theta_{cap} \\ 0 & \text{if } \bar{\theta} \leq \theta_{pwp} \end{cases} \qquad (13)$$

$$f_3(D_a)^{-1} = \exp(-g_D.D_a) \qquad D_a = e_{sat}(T_a) - e(T_a) \qquad (14)$$

e is vapour pressure.

Soil surface resistance

A separate formulation is used for bare soil. In this case relationship (Eq 11) is not used and is replaced by Eq 15. A minimum stomatal resistance is associated to bare soil (Table 1) to represent the minimum soil resistance and the only stress assumed for soil evaporation is due to soil water deficit, via a modified Jarvis function $f_{2,BS}$ which allows a broader range of soil moisture sensitivity (Eq 16).

$$r_c = r_{s,min} . f_{2,BS}(f_{liq}.\theta_1) \qquad (15)$$

$$f_{2,BS}(\bar{\theta})^{-1} = 1 + \\ \exp\left(-50. \frac{\theta - \theta_{PWP}}{1000.(\theta_{fc} - \theta_{pwp}) + 1} \right) \qquad (16)$$

Wet canopy evaporation

In case of wet canopy, evaporation of the wet fraction is not calculated separately from vegetation tiles. A wet fraction is determined from relative air humidity and LAI (Eq 17). The relations have been built upon analysis of the interception reservoir and concurrent relative humidity of one year of ECMWF IFS (Ghilain et al, 2017). The stomatal resistance of the vegetation is modulated by the fraction of dry canopy: $R_s=(1-F_{wet}).R_{s,veg}$. It assumes that the stomatal resistance of water interception is zero (like for open water), while the aerodynamic resistance is driven by roughness lengths from the underlying vegetation. It has been shown to be similar to calculating as an additional tile in the iterative process, but involves less complexity in the code.

(Day) If $Rh_{a, 2m} >= 81\%$, (Night) If $Rh_{a, 2m} >= 88\%$, (17)

$$F_{wet} = \frac{\min(0.0002.Rh^3 - 0.0414.Rh^2 + 3.3850.Rh - 92.6421, 0.5)}{0.2.LAI}$$

$$F_{wet} = \frac{\min(0.003.Rh^2 + 0.4833.Rh + 19.5359, 0.5)}{0.2.LAI}$$

Anthropogenic surface heat flux

For cities, sensible heat flux (Eq 18) is the sum of the sensible heat flux caused by meteorological processes and an additional sensible heat flux resulting from human activities H_{anthro}, which is evaluated on the basis of a climatology derived by Flanner (2009). It includes latitudinal (θ), seasonal (W_y) and diurnal variations (W_d).

$$H_{anthro} = \overline{H}_{anthro}.W_d(t_d).W_y(t_y) \quad (18)$$

$$W_d = E_1.b_1 + H(t_d).E_1.E_2 + b_2$$

$$H(t_d) = A_1.\cos(2\pi.t_d)$$

$$E_{1/2} = 0.5.erf(\pm\alpha.(t_d - \mu \pm \varepsilon)/\sigma) + 1$$

$$W_y(t_y) = 1 + A_2(\theta).\sin(2\pi(t_y + 0.25))$$

$t_{d/y}$ is the fractional time of day/year, $b_1 = 0.451$, $b_2 = 0.8$, $\sigma = 0.18$, $\mu = 0.5$, $A_1 = -0.3$, $f = 2$, $\alpha = 10$, $\varepsilon = 0.25$.
$A_2 = \pm(1 - e^{\mp(\theta \mp 33)/25})$ $\theta > 33; \theta < -33$; $A_2 = 1$ otherwise

Fire events

In case of fire, the energy balance does not obey anymore the same physical laws, as the heat is generated from the burning of biomass. LSA-SAF FRP Pixel product is used to localize and to help derive heat fluxes in such events (Eq 19). During a fire event, all the tiles are considered to participate to the burning process. Live fuel moisture content is empirically estimated from the day of the year (*doy*), skin temperature and FVC, adapted from Chuvieco et al (2004), and parametrized differently for low (TVL) and high vegetation tiles (TVH).

$$H = c.FRP.\beta_l.h.(1 - B)$$

$$LE = c.FRP.\beta_l.L_v.(B + 0.56.(1 - B))$$

$$B = \frac{LFMC}{LFMC + 1} \quad (19)$$

$$LFMC = l_1 - l_2.T_{sk} + l_3.FVC + l_4.FD$$

$$FD_{TVL} = (\sin(1.5.\pi.(doy + doy^{1/3})/365))^4).1.3$$

$$FD_{TVH} = ((\sin(1.5.\pi.doy/365))^2) + 1).0.35$$

$c = 0.368$ kg.MJ^{-1} (Wooster et al, 2005)
$h = 17.5$ MJ.kg^{-1} ()
(TVL) $l_1 = -57.1$, $l_2 = -0.09$, $l_3 = 284.81$, $l_4 = 136.75$
(TVH) $l_1 = 70.19$, $l_2 = -1.43$, $l_3 = 53.52$, $l_4 = 122.09$
(Chuvieco et al, 2004)
β_l are defined in Table 1 (Kaiser et al, 2012)

Instantaneous products

Surface heat flux values for the whole pixel are calculated as a weighted contribution of each tile. ζ_i is the fraction of i tile in pixel (Eq 20).

$$LE = \sum \zeta_i LE_i \quad (20)$$

$$H = \sum \zeta_i H_i$$

The LE obtained for the whole pixel is expressed in W.m^{-2}. The corresponding evapotranspiration values, expressed in mm.h^{-1}, are given by Eq 21.

$$ET = 3600.LE/L_v \quad (21)$$

Latent heat of vaporization (L_v) (Eq 22) is $\qquad L_v = [2.501\text{-}0.00234\ (T_a - 273.15)]\ 10^6$ $\quad$ (22)

On snow tiles, the latent heat of sublimation is used ($L_s = L_f + L_v$, $L_f = 334 kJ.kg^{-1}$).

Iterative solver and time step organization

Solving the system of equations requires an iterative method, because of the non-linear inter-dependence of the variables H, LE, T_{sk} and u_*. In the ET implementation, a single point iteration method has been selected for solving the system of equations, assuming neutral stability as initial condition. Iteration is stopped when pixel estimates of the three key-variables (H, LE, T_{sk}) are stabilized, using a predefined precision (difference between two successive iteration less than 0.1 for H and LE and 0.01 for T_{sk}) criterion. When the number of iterations exceeds 100, the process is stopped and algorithm returns the flag 'not-converged'.
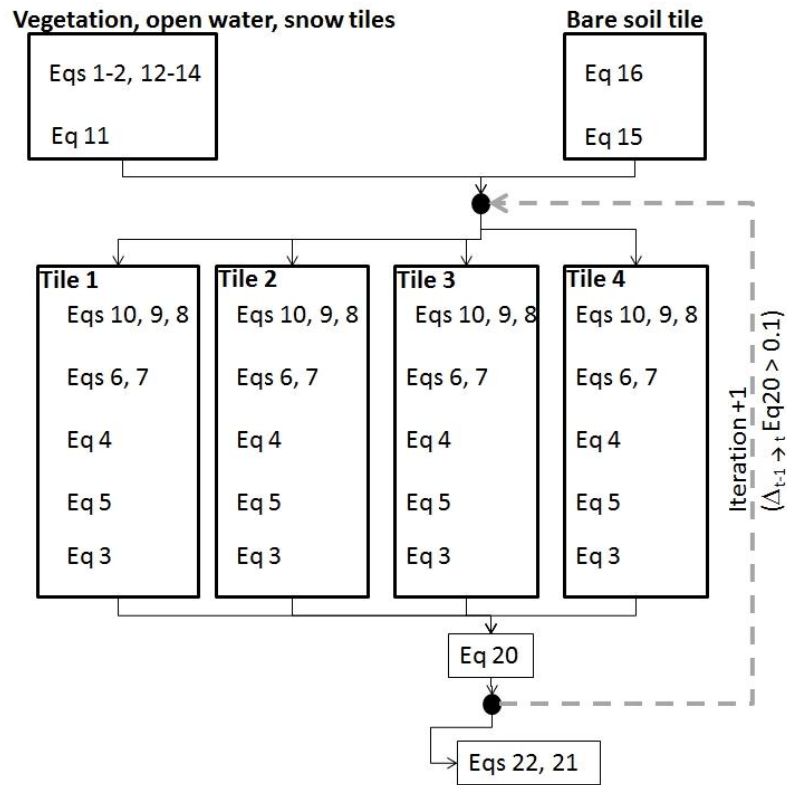
Figure 5: Flowchart illustration of the iterative solving process. The central blocks correspond to the 4 dominant tiles per pixel. The iteration is done until convergence of the pixel averaged values of H, LE and Tskin.

2.3 Post-processing: daily evapotranspiration production

Daily evapotranspiration is obtained by temporal integration of instantaneous values generated by the MET algorithm according to

$$DMET = \int_{h_1}^{h_2} ET_i(t)dt \tag{23}$$

where ET_i are the instantaneous evapotranspiration estimated provided by the MET algorithm every 30 minutes for a given day. The integration limits ($h1$, $h2$) correspond to the first (theoretically at 00:30 UTC) and last (theoretically at 24:00 UTC) existing slots for a given day. In the best situation, a total of 48 images are generated by day. It means that for each MSG pixel, 48 ET values have to be integrated. It happens that some images are missing for a given day. In order to provide a daily consistent value for each pixel, a linear interpolation between the closest slots is applied according to

$$ET_{gap=before+1\rightarrow after-1} = 0.5\,(ET_{after} + ET_{before})\,N \tag{24}$$

where ET_{before} and ET_{after} are previous and next existing ET values for the same pixel in considered day and N is the number of time steps between previous and next existing ET values. The underlying assumption is that missing calculations are not situation specific and are randomly distributed. The information on the number of missing slots is included in the metadata of the LSA-SAF DMET product.

3 Product description

The MET v2 algorithm produces evapotranspiration estimates in mm.h^{-1} over the full MSG disk (four LSA-SAF defined windows) at MSG/SEVIRI spatial resolution with a 30 minutes time step. Together with the ET map, a quality flag image is also generated. This image has the same size as the ET image and provides information on pixel-by-pixel basis. It informs about the quality of input variables and if pre/post-processing (gap filling) was performed on input or output data. Every 30 minutes is generated a file containing maps of H, LE and G with their associated quality flag.

DMET product is provided along with 2 images informing about the number of missing slots and the percentage of missing values pixel by pixel.

4 Global quality and added value of ET v2 and surface heat fluxes

Global quality: theoretical considerations and preliminary validation

The LSA-SAF ET v2 suite proposes integrated products from the LSA-SAF: sensible, latent and ground heat fluxes. Those fluxes provide the necessary terms to complement the energy balance and partition of the net radiation terms already available from LSA-SAF (DSSF, DSLF, AL, EM, LST); the evapotranspiration products provide necessary information to complete the water cycle. The prototype of LSA-SAF ET v2 has been extensively validated over more than 30 ground reference sites over Europe and Africa. Results provide confidence that the LSA-SAF ET is robust and capable of reproducing ET estimates with a range of uncertainty slightly larger than measurements uncertainty (Ghilain et al, 2015b)[2]. Detailed validation results will be presented in a companion Validation Report.

Based on the current results, we conclude that the performances of the algorithm are in general very good over Europe and for Africa. Over South America, no observation allows us in the present time to be absolutely confident of the results provided, but further validation effort will be pursued and reported in the subsequent validation reports.

Added value of the LSA-SAF ET products within the community effort

Advantages of LSA-SAF ET v2

---

[2] Results based on the comparison of a prototype of the 1D algorithm and the observations from in-situ eddy covariances systems over 96 sites-years across Europe and Africa.

1 – An uniform applicability to continental scales

2 – A production in near-real time

3 – A production for all weather conditions

4 – A generation at high frequency (30 min)

5 – A few kilometres spatial resolution

6 – A daily ET as integration of potentially 48 images

7 – A model mostly driven by remote sensing data

8 - An easier comparison with ground reference thanks to the 'tile' approach

9 – Enhanced capabilities compared to simple algorithms

LSA-SAF ET v2 provides products more in line with the requirements of the modelling community, lessening the dependency to NWP outputs in assimilating more satellite derived data. However, the algorithm can be viewed as an information system based on a tri-axial combination of modelling-forecast-remote sensing. It is therefore not a "pure" remote sensing product, totally independent from NWP output. As such, LSA-SAF ET v2 is not independent from ECMWF IFS or land analyses (eg H-SAF SM-DAS-2), but provides tailored products assimilating additional satellite products in near-real time, while providing continuity and stability over time and in-taking recent advances put in operations at ECMWF.

In terms of the spatial and temporal resolution, the LSA-SAF ET v2 products should be useful for water and agriculture management scientists and some climate scientists, while the near-real time availability is expected to meet the demand of 28% of the scientific community of users that absolutely requires this information in due time (WACMOS-ET user inquiry).

With its characteristics, LSA-SAF ET v2 could perfectly nest in initiatives arising from GEWEX LandFlux to build a global composite ET dataset (WACMOS-ET Road map) and some steps have already been taken into that direction.

Limitation of the LSA-SAF ET&SF algorithm and possible ways forward

The algorithm presented here has been especially designed for the near-real time services. The involved methods are consequently targeting this use for optimality. Although the resulting products may be useful in the context of analyses over period of several years (eg Ghilain et al, 2015), choices in the algorithm may be sub-optimal for users targeting climate analyses, as for example there is no feedback possible between the surface and the underlying soil. The parameterization used for calculation of the surface properties (eg roughness lengths, minimum canopy resistance, phase and amplitude of the heat storage capacity) bears some uncertainty, that may be reduced in future releases, by means of a more precise parameterization (eg Su, 2002 for roughness lengths) or better modelling of respiration and photosynthetic activity (eg Calvet et al, 1998, Carrer et al, 2013).

Expected improvement of the LSA-SAF ET v2 products compared to operational LSA-SAF ET

For temperate regions, a neutral impact is expected, except from a slight improvement of the seasonal dynamics over agricultural lands and over forests after rainfall events.

A strong positive impact is expected in arid and semi-arid regions. This is due to the assimilation of additional remote sensing derived products related to vegetation and soil moisture status, and to an improved parameterization of the bare soil evaporation. Especially,

we point the fact that irrigation is indirectly taken into account by using satellite information in the thermal infra-red bands.

5   References

Albergel, C., Balsamo, G., de Rosnay, P., Muñoz-Sabater, J., and Boussetta, S., 2012: A bare ground evaporation revision in the ECMWF land-surface scheme: evaluation of its impact using ground soil moisture and satellite microwave data, Hydrol. Earth Syst. Sci., 16, 3607-3620, doi:10.5194/hess-16-3607-2012.

Arboleda A., Ghilain N., Gellens-Meulenberghs F., 2015: Prospective changes in the LSA-SAF evapotranspiration products, Poster presented at the 6th LSA-SAF user workshop, 6-8 June 2015, Reading, UK.

Arboleda A., Ghilain N., Gellens-Meulenberghs F., 2011: EUMETSAT's LSA-SAF evapotranspiration: comparisons of operational product to observations and models at hydrological basins scale, 7 p., Proceedings of the EUMETSAT conference, September 2011, Oslo, Norway.

Balsamo G, Viterbo P, Beljaars A, van den Hurk B, Hirschi M, Betts AK, Scipal K. 2009. A revised Hydrology for the ECMWF model: verification from field site to terrestrial water storage and impact in the integrated forecast system. Journal of Hydrometeorology, 10:623–643.

Bastiaassen, W.G.M. 1995. Regionalization of surface flux densities and moisture indicators in composite terrain. Ph.D. thesis, SC-DLO, Wageningen, The Netherlands. 271pp.

Beljaars A.C.M., Viterbo P., 1994: The sensitivity of winter evaporation to the formulation of aerodynamic resistance in the ECMWF model, *Boundary-Layer Meteorol. Vol. 71, pp. 135-149.*

Calvet, J.-C., J. Noilhan, J.-L. Roujean, P. Bessemoulin, M. Cabelguenne, A. Olioso, and J.-P. Wigneron, 1998. An interactive vegetation SVAT model tested against data from six contrasting sites, Agric. For.Meteorol.,92,73–95.

Carrer, D., Roujean, J.-L., Lafont, S., Calvet, J.-C., Boone, A., Decharme, B., Delire, C., and Gastellu-Etchegorry, J.-P., 2013: A canopy radiative transfer scheme with explicit FAPAR for the interactive vegetation model ISBA-A-gs: Impact on carbon fluxes, J. Geophys. Res., 188, 888–903.

Chehbouni, A., Lo Seen, D. , Njoku, E.G. and Monteny, B. 1996. A Coupled Hydrological and Ecological modeling Approach to examine the Relationship between Radiative and Aerodynamic Surface Temperature over Sparsely Vegetated Surfaces. Remote Sensing Environment.

Choudury B.J., Idso S.B., Reginato J.R., 1987: Analysis of an empirical model for soil heat flux under a growing wheat crop for estimating evaporation by an infrared-temperature based energy balance equation, *Agr. For. Meteorol., 39, pp. 283-297.*

Choudhury,B.J.,1991: Multi spectral satellite data in the context of land surface heat balance, Rev.Geophys, 29, pp. 217-236.

Chuvieco E., Cocero D., Aguado I., Palacios A., Prado E., 2004: Improving burning efficiency estimates through satellite assessment of fuel moisture content, J. Geophys. Res., 109, D14S07, doi:10.1029/2003JD003467.

Courault D., Seguin B. and A. Olioso, 2005: Review on estimation of evapotranspiration from remote sensing data: from empirical to numerical modelling approaches, *Irrigation and Drainage Systems Vol. 19, pp. 223-249.*

Faroux, S., Kaptué Tchuenté, A. T., Roujean, J.-L., Masson, V., Martin, E., and Le Moigne, P., 2013: ECOCLIMAP-II/Europe: a twofold database of ecosystems and surface parameters at 1 km resolution based on satellite information for use in land surface, meteorological and climate models, Geosci. Model Dev., 6, 563-582, doi:10.5194/gmd-6-563-2013.

Flanner M. G., 2009: Integrating anthropogenic heat flux with global climate models, Geophys. Res. Lett., **36**, L02801, doi:10.1029/2008GL036465.

Friedl, M.A., 2002, Forward and inverse modeling of land surface energy balance using surface temperature measurements. Remote Sens Environ, 79, pp. 344–354.

Ghilain N., Arboleda A. and Gellens-Meulenberghs F., 2011: Evapotranspiration modelling at large scale using near-real time MSG SEVIRI derived data, Hydrol. Earth Syst. Sci., 15, pp. 771-786, doi:10.5194/hess-15-771-2011.

Ghilain N., Arboleda A., Sepulcre-Cantò G., Batelaan O., Ardö J. and Gellens-Meulenberghs F., 2012: Improving evapotranspiration in a land surface model using biophysical variables derived from MSG/SEVIRI satellite. *Hydrol Earth Syst Sci*, 16(8), pp.2567-2583.

Ghilain N., Arboleda A., Batelaan O., Trigo I., Ardö J., Gellens-Meulenberghs F., 2016: Tracking down Eart surface moisture: fulfilling the promise of geostationary satellites, Remote Sens Environ, in review.

Ghilain N., Arboleda A., Gellens-Meulenberghs F., 2015: Continental scale monitoring of (sub-) daily evapotranspiration enhanced by the assimilation of geostationary data, poster presented at the GEWEX ESA workshop on Earth Observation of the water cycle, 21-23 October 2015, Frascati, Italy.

Ghilain N., Arboleda A., Barrios J. M., Gellens-Meulenberghs, F., 2017: Water interception by canopies for remote sensing based evapotranspiration models, in preparation.

Hasenauer, S., 2010: Bias correction of soil moisture time series from ERS scatterometer and ERA-Interim data for a global 10-year period, 2010 EUMETSAT Meteorological Satellite Conference, 8 pp.

Helman, D., Lensky, I. M., and Givati, A., 2015: Annual evapotranspiration retrieved solely from satellites' vegetation indices for the Eastern Mediterranean, Atmos. Chem. Phys. Discuss., 15, 15397-15429, doi:10.5194/acpd-15-15397-2015.

Hu, G., Jia, L., & Menenti, M.: Comparison of MOD16 and LSA-SAF MSG evapotranspiration products over Europe for 2011, Remote Sens. Environ., 156, 510-526, 2015.

Jacobsen A, Hansen BU., 1999: Estimation of the soil heat flux/net radiation ratio based on spectral vegetation indexes in high-latitude Arctic areas. *Int J Remote Sensing,* **20**, pp. 445–461.

Jovanovic, N., Garcia, C. L., Bugan, R. D., Teich, I., & Rodriguez, C. M. G., 2014: Validation of remotely-sensed evapotranspiration and NDWI using ground measurements at Riverlands, South Africa, Water SA, 40(2), 211-220.

Kaiser, J. W., Heil, A., Andreae, M. O., Benedetti, A., Chubarova, N., Jones, L., Morcrette, J.-J., Razinger, M., Schultz, M. G., Suttie, M., and van der Werf, G. R., 2012: Biomass burning emissions estimated with a global fire assimilation system based on observed fire radiative power, Biogeosciences, 9, 527-554, doi:10.5194/bg-9-527-2012.

Kustas, W. P., C. S. T. Daughtry, and P. J. Van Oevelen, 1993: Analytical treatment of the relationships between soil heat flux/net radiation ratio and vegetation indices. *Remote Sens. Environ.*, **46,** 319-330.

Liou Y-A and Kumar Kar, S., 2014: Evapotranspiration estimation with remote sensing and various surface energy balance algorithms – a review, Energies, **7**, 2821-2849.

Martins J., Trigo I., Ghilain N., Goettsche F., Olesen F., Meulenberghs F., Arboleda A., 2016: Feasibility study of an all-weather land surface temperature product, 2016 EUMETSAT conference, Darmstadt, Germany, September 2016.

Masson, V., Champeaux, J. L., Chauvin, F., Meriguet, Ch. and Lacaze, R. A., 2003. Global Database of Land Surface Parameters at 1-km Resolution in Meteorological and Climate Models. *J. Climate 16(9), 1261-1282*.

Norman J.M., Kustas W.P., Humes K.S., 1995: A two-source approach for estimating soil and vegetation energy fluxes from observations of directional radiometric surface temperature, Agr. For. Meteorol., 77, pp. 263-293.

Peel M. C., Finlayson B. L., McMahon T. A., 2007: Updated world map of the Köppen-Geiger climate classification, Hydrol. Earth Syst. Sci., 11, pp. 1633-1644.

Petropoulos, G.P., G. Ireland, A. Cass & P.K. Srivastava, 2015: Performance Assessment of the SEVIRI Evapotranspiration Operational Product: Results Over Diverse Mediterranean Ecosystems IEEE Sensors, [in press], DOI 10.1109/JSEN.2015.2390031.

Petropoulos G.P., 2013: Remote Sensing of Surface Turbulent Energy Fluxes. Chapter 3, pages 49-84, in "Remote Sensing of Energy Fluxes and Soil Moisture Content ", by G.P. Petropoulos, Taylor and Francis, ISBN: 978-1-4665-0578-0.

Santanello and Friedl, 2003: Diurnal covariation in soil heat flux and net radiation, *J. Appl. Meteorol., 42, pp. 851-862*.

Siebert, S., Henrich, V., Frenken, K., Burke, J., 2013: Update of the Global Map of Irrigation Areas to version 5, FAO Project report, 178 p.

Simard, M., N. Pinto, J. B. Fisher, and A. Baccini, 2011: Mapping forest canopy height globally with spaceborne lidar, J. Geophys. Res., 116, G04021, doi:10.1029/2011JG001708.

Su, Z., 2002: The Surface Energy Balance System (SEBS) for estimation of turbulent heat fluxes, Hydrol. Earth Syst. Sci., 6, 85-100, doi:10.5194/hess-6-85-2002.

Trigo, I. F., DaCamara, C. C., Viterbo, P., Roujean, J.-L., Olesen, F., Barroso, C., de Coca, F. C., Carrer, D., Freitas, S. C., Garcia-Haro, J., Geiger, B., Gellens-Meulenberghs, F., Ghilain, N., Melia, J., Pessanha, L., Siljamo, N., & Arboleda, A., 2011: The Satellite Application Facility on Land Surface Analysis, Int. J. Remote Sens., 32 , 2725-2744.

Van den Hurk, B., Viterbo, P., Beljaars, A. and Betts, A., 2000: Offline validation of the ERA40 surface scheme. *ECMWF Techn. Memorandum No.295, 42 pp*.

Verstraeten, W.W.; Veroustraete, F.; Feyen, J., 2008: Assessment of Evapotranspiration and Soil Moisture Content Across Different Scales of Observation, *Sensors, , 8*, pp. 70-117.

Viterbo, P. and Beljaars, A., 1995. An improved surface parameterization scheme in the ECMWF model and its validation. *J. Climate 8, 2716-2748*.

WACMOS ET users inquiry, accessible online (accessed 9/11/2015): http://aramis.obspm.fr/~jimenez/Docs/WACMOSET/WACMOSET_WP1100_approved.pdf

WACMOS ET Road map, accessible on-line (accessed 9/11/2015): http://aramis.obspm.fr/~jimenez/Docs/WACMOSET/WACMOSET_WP3300_approved.pdf

Wang K. and Dickinson, R. E., 2012: A review of global terrestrial evapotranspiration: observation, modelling, climatology, and climatic variability, Rev. Geophys., 50, RG2005, doi:10.1029/2011RG000373.

Wooster, M. J., Roberts G., Perry G. L. W., Kaufman Y. J., 2005: Retrieval of biomass combustion rates and totals from fire radiative power observations: FRP derivation and calibration relationships between biomass consumption and fire radiative energy release, J. Geophys. Res., 110, D24311, doi:10.1029/2005JD006318.

Algorithm Theoretical Baseline Document (ATBD), H-SAF H14 Product – SM-DAS-2 – Soil Wetness Index in the roots region, version 0.2, September 2011, 41 pp.

6   Annexes

Annex A: Production of static input files for use in the algorithm

Land cover map   ECOCLIMAP-I/II (Masson et al., 2003; Faroux et al, 2013) gives a land cover classification in terms of 11 elementary classes, associated to the 10 land cover types adopted for the evapotranspiration algorithm, including water that is used in wetland landscapes (Table 4). ECOCLIMAP-I/II land cover map is aggregated to SEVIRI resolution: the fraction of each tile within every pixel is retrieved. The fixed fraction of bare soil includes only clearly identified bare soil areas, excluding rocks and urban material that are treated separately. The FAO lithology map is used to refine the distinction between bare soil and rocky soils. Identification of organic soils enables the selection of the conversion factor in case of fire.

Table 4: ECOCLIMAP tiles associated to LSA-SAF-ET model tiles.

#	LSA-SAF ET v2 algorithm	ECOCLIMAP
1	Bare soil	Bare soil
2	Snow	Permanent snow
3	Deciduous Broadleaved trees	Deciduous broadleaf trees
4	Evergreen Needleleaved trees	Evergreen needleleaved trees
5	Evergreen Broadleaved trees	Evergreen broadleaved trees
6	Crops (2 types)	C3 and C4 crops
7	Irrigated crops	Irrigated crops
8	Grass (2 types)	Natural herbaceous not irrigated
9	Bogs and Marshes	Swamp herbaceous and gardens
10	Rocks	Rocks
11	Open water	Water
12	City	Urban

Biophysical variables   The evapotranspiration algorithm requires continuous LAI input at tile level. LSA-SAF provides a daily LAI product, at SEVIRI spatial resolution. A method has then been designed to build continuous LAI fields based on an optimal interpolation between a 10-days climatology constructed on a 4-years dataset and the actual daily product (Ghilain et al., 2012). Therefore, a map for each 10-days period of the year of LAI and albedo averages is stored in the static file, with an errorbar, computed as the standard deviation of the sample, used for the assimilation algorithm.

Soil moisture parameters   A mask, based on the results of an in-situ comparison (Arboleda et al, 2015), a climate classification map (Köppen-Geiger, Peel et al, 2007), orography map (GTOPO) and potentially irrigated areas (FAO GIAM, Siebert et al, 2013), is available to select the source of soil moisture input. In addition, maps of soil moisture conditions based on 5 years LST data (2010-2015) and the per-pixel parameters of the fit (CDF matching) between ECMWF IFS SWVL1/H-SAF SM-DAS-2 H14 and soil moisture derived from LST are provided. The CDF matching is based on the method described in Hasenauer (2010). It is a linear transformation of the modelled soil moisture into the needed soil moisture. Orography map is used to screen the regions where LST is affected by problems of illumination and sensor viewing geometry. The slopes from the DEM map are calculated based on neighbouring pixels, and a threshold is set.

Table 5: Layers of the static file generated at RMI, Belgium, and transferred to the LSA-SAF operational centre at IPMA, Portugal.

Themes	Layers	#
Land cover	Land-Water mask	1
	Tile number	5
	Tile fraction	5
	FAO lithology	1
	FAO soil	1
Vegetation	LAI (10 days)+err	72
	Albedo (10 days)+err	72
Soil moisture	Selection input	1
	CDF matching coefficients	4
	Extrema heating rates	2
	Anisotropy corrective parameters	2

Annex B: Added-value of algorithm v2 compared to the v1

More remote sensing data to better drive the physical model   Successive validation exercises have demonstrated that v1 has a good value in monitoring ET (Ghilain et al, 2011; Arboleda et al, 2012; Hu et al, 2015; Petropoulos et al, 2014; Petropoulos et al, 2015; Jovanovic et al, 2014). However, evidences of some limitations have been reported, especially over semi-arid Africa and in some areas of Southern Europe (LSA-SAF ET VR; Helman et al, 2015). Most of the reports lead to the conclusion of an inadequate soil moisture input used in the ET algorithm, due either to a relative instability over time due to change of operational cycles at ECMWF affecting the predicted soil moisture or to an inadequacy of spatial resolutions or accuracy of the input from ECMWF forecasts. As vegetation dynamics is closely linked to soil moisture availability, it has been considered in the same time. First, the ET algorithm v2 has been conceived to assimilate the daily vegetation characteristics to fully exploit the capabilities of LSA-SAF vegetation products to monitor short term drops due to sudden damages (eg fire disturbance, clear cutting forests, hail) and inter-annual variability. Then, the soil moisture input has been revised such as to integrate more remote sensing data into play in critical regions where soil water availability is highly variable and difficult to predict from forecasting systems. In that respect, the soil moisture dynamics in v2 is better represented in drylands, irrigated areas, lowlands, wetlands thanks to the use of the temporal variation of the land surface temperature in selected areas. Also, the impact of the change of operational cycles could be reduced if the H-SAF product root-zone soil moisture is used, as it is more stable over time and not affected by changes of operational cycles.

Improved parameterizations for a better accuracy   The parameterization of the environmental constrains on evapotranspiration rates has been improved for low vegetation classes in conditions of low coverage and for bare soil.

New effects of snow, urban activities, rain and fire activity   In v1, snow effect and rain evaporation was not considered. In v2, snow cover is taken into account, when it is permanent and when temporary and visible with SEVIRI (clear sky), and rain evaporation is modelled, when rain deposition on leaves is detected in the ECMWF forecasts (thresholding technique on the ECMWF forecastd relative humidity of the air). Thermal efects of the urban activities are now reflected in the product, and especially in the sensible heat flux by means of a bulk parameterization and in the evapotranspiration taking into account the imperviousness of urban

areas. In case of fire, v2 makes use of a dedicated algorithm that convert the burning biomass evaporative potential in instantaneous fluxes of water and turbulent energy. All in all, a better representation of the different components of evapotranspiration should better reflect the spatial variability of the evapotranspiration.

7 List of acronyms

AL-BB-BH	Bi-hemispherical Broadband Albedo
AOD	Aerosol Optical Depth
CDF	Cumulative Distribution Function
DMET	Daily MSG evapotranspiration
DSLF	Downwelling Surface Longwave Flux
DSSF	Downwelling Surface Shortwave Flux
ECMWF	European Center for Medium-range Weather Forecasts
ET	Evapotranspiration
EMMAPS	Emissivity of the land surface
FAO	Food and Agriculture Organization
FRP	Fire Radiative Power
GEWEX	Global Energy and Water Cycle Exchanges Project
H	Surface sensible heat flux
HR	Heating rate
H-SAF	Satellite Application Facility on Hydrology
IFS	Integrated Forecast System
LAI	Leaf Area Index
LE	Surface Latent Heat flux
LSA-SAF	Satellite Application Facility on Land Surface Analysis
MACC	Copernicus Atmospheric Monitoring Service
MET	MSG Evapotranspiration
MSG	Meteosat Second Generation
NWP	Numerical Weather Prediction
SEVIRI	Spinning Enhanced Visible and InfraRed Imager
SLP	Sea Level Pressure
SM-DAS-2	Soil moisture Data Assimilation System -2
SRS	Satellite Remote Sensing
SSM	Surface soil moisture
SVAT	Soil-Vegetation-Atmosphere Transfer
STL	Soil Temperature for a specific soil layer
SWVL	Soil Water Volumetric content for a specific soil layer
TESSEL	Tiled *ECMWF* Scheme for Surface Exchanges over Land
TIR	Thermal InfraRed
VR	Validation Report
10U	X component of the wind vector at10 m above the surface
10V	Y component of the wind vector at10 m above the surface
2T	Air temperature at 2 m above the surface
2D	Dew point temperature at 2 m above the surface

8 Developers

The method has been developed, designed and software coded in fortran at the Royal Meteorological Institute of Belgium (RMI) by Alirio Arboleda, Nicolas Ghilain and Françoise Meulenberghs. The software will be delivered to the LSA-SAF operational centre at IPMA, Portugal.